Available online at www.sciencedirect.com
ScienceDirect
International Journal of Multiphase Flow 33 (2007) 742–765
International Journal of Multiphase Flow
www.elsevier.com/locate/ijmulflow

Experimental and numerical analysis of high pressure diesel spray–wall interaction

L. Andreassi [a], S. Ubertini [a,*], L. Allocca [b]

[a] Department of Mechanical Engineering, University of Rome "Tor Vergata", Via del politecnico, 1-Roma, Italy
[b] Istituto Motori, CNR, Via Marconi, 8-80125 Napoli, Italy

Received 1 June 2006; received in revised form 8 January 2007

Abstract

The interaction between impacting and splashed droplets and air motion plays a fundamental role on the mixture formation process, which is a crucial aspect for the correct operation of modern DI Diesel engines as it greatly influences the combustion process and the exhaust emissions. A complete understanding of spray impingement is quite complex. A mixed numerical–experimental approach is proposed in this paper.

The experimental tests are carried out with a high pressure (up to 120 MPa) diesel spray emerging from an axial disposed single-hole nozzle in an optically accessible vessel, pressurized up to 5.0 MPa at ambient temperature. The jet impacts on a flat stainless steel wall heated up to 500 °C by a 200 W temperature regulated electrical resistance wire. The experimental analysis is performed using a Bosh tube as the injection mass flow meter, a pulsed laser sheet generated on the second harmonic of a Nd-YAG laser and a synchronized CCD camera. Digital image post-processing allows extraction of the radial penetration and thickness growth of the impacted fuel versus injection pressure, vessel back-pressure and wall temperature. Moreover, a procedure to relate light intensity to average fuel density is proposed.

The numerical analysis is carried out by means of a multi-dimensional numerical tool, based on the KIVA-3V code. The spray–wall interaction is simulated through a phenomenological splash model available in literature and validated for low injection pressures (up to 300 bar) and ambient back-pressure. The comparison between experimental and numerical results demonstrates the inability of the model in predicting high pressure spray–wall interaction, especially under increasing back-pressures. Based on the experimental evidences, a modified version of the model is proposed and the new model is proven to be an adequate representation for different injection pressures and back-pressures.

Keywords: High pressure diesel spray; Spray/wall interaction; Splash model; Digital image post-processing; Multi-dimensional numerical tool

* Corresponding author. Tel.: +390672597170; fax: +390623310028.
E-mail address: stefano.ubertini@uniroma2.it (S. Ubertini).

0301-9322/$ - see front matter © 2007 Elsevier Ltd. All rights reserved.
doi:10.1016/j.ijmultiphaseflow.2007.01.003

1. Introduction

The development of compact high-speed direct-injection Diesel engines has stimulated the interest on the phenomena associated with impact of sprays on solid walls. Due to the short distance between the injection nozzle and the piston head, and the high injection pressures, the fuel spray may impinge on engine surfaces before it is fully vaporized and mixed with air. Accordingly, spray–wall interaction becomes an unavoidable and important phenomenon as the behaviour of the impinging spray has a great influence on the fuel dispersion, evaporation, mixture formation, combustion process and exhaust emissions. It has been experimentally demonstrated that soot levels under Diesel engine-like operating conditions (injection pressure = 1380 bar, back-pressure = 42 bar) are lower for wall jets than for free jets. This effect is related to the enhanced mixing with air, which favours soot oxidation, and to the jet cooling by the wall (Lopez and Pickett, 2004).

The spray impingement process involves three physical phases (droplet, wall and gas in the near-wall region) and two main physical processes (wall spray development and wall film evolution), being influenced by parameters related to both physical and kinematics properties of the impinging droplets. A complete understanding of spray–wall interaction is, therefore, complex and requires a combined experimental and numerical approach to obtain a detailed knowledge of all the processes involved.

Spray–wall interaction is difficult to analyze experimentally, especially for the high fuel density and injection velocity that are typical in modern Diesel injection systems. Consequently, data are very poor, challenging and expensive to obtain and most of the experiments reported in literature are carried out in simplified laboratory configurations (Katsura et al., 1989; Saito et al., 1993; Fujimoto et al., 1990; Arcoumanis and Chang, 1994; De Vita et al., 2002; Di Stasio et al., 2000; Allocca et al., 1993, 2002; Amagai and Arai, 2004; Winterbone, 1994).

Other studies are related to single droplet impingement in simplified geometries and for different wall temperatures (Mills and Fry, 1982; Xiong and Yuen, 1991). Some authors have considered the nature of the surface (Wu, 1992; Mundo et al., 1995) while others have studied the secondary atomization produced by the impact of the single droplet on a heated surface (Cossali et al., 2005). The characterization of the behaviour of a single droplet impacting on a heated plate is strongly related to different boiling conditions observed at increasing surface temperature (T_w). The temperature of the wall produces "wetting", "transition" and "non-wetting" regimes depending on Nukiyama and Leidenfrost fuel characteristic temperatures (Moita and Moreira, 2005).

On the other hand, computational modelling offers a promising opportunity to obtain detailed information on the spray–wall impingement and wall-film build-up. Although many numerical research studies are available, the proposed models have not yet been tested at high injection pressures typical of modern DI diesel engines.

One of the first numerical formulations was presented by Naber and Reitz (1988) who used the results of Wachters and Westerling (1966) to define a droplet–wall interaction model to be linked to a multi-dimensional code. This model was further extended by Allocca et al. (1990), who took into account droplets atomization, and by Eckause and Reitz (1995), who investigated the heat transfer during impingement, and by Guerrassi and Champoussin (1996), who proposed the use of probability functions to calculate the secondary droplet diameters and normal velocities. Another significant study was performed by Wang and Watkins (1993), who defined a new droplet-wall impingement model implemented in a two-phase CFD code. Their model could correctly predict the wall–spray radius but its height was underpredicted for all the analysed test-cases. One of the most interesting studies was performed by Mundo et al. (1995, 1996), who use empirical correlations given in the form of exponential or polynomial functions. Subsequently, Marengo et al. (1996) improved this numerical model by incorporating the effects of wall film thickness on the splash regime. Based on the splash criteria defined by Mundo et al. (1995), Grover and Assanis (2001) introduced a new splash model into the KIVA-3V code. Their model is based on the conservation of mass, tangential velocity and kinetic energy and uses specific criteria to make a distinction between dry and wetted surface. Furthermore, the model incorporates a viscous dissipation effect and it discriminates between viscous dissipation and wall film formation to characterize the energy loss. The submodel proposed by Stanton and Rutland (1996) is also based on the experimental data of Mundo et al. (1995) and involves the liquid film model and the splash effect, in which the ejection angle is uniformly determined from linear interpolation of the experimental data. Also Yarin and Weiss (1995) performed a mixed experimental–numerical study on the splash phenomenon, showing that

this effect corresponds to the velocity discontinuity occurring between the fluid moving outward from the splash location and slower fluid on the wall. In this research, they did not observe a correlation between incident droplet size and normal velocity, as, on the contrary, remarked by Mundo et al. (1995). Bai and Gosman (1995) developed a model that solves the conservation of energy of an impinging parcel and employs a number of assumptions derived from experimental data. More recently O'Rourke and Amsden (1996, 2000) incorporated a new model in the KIVA code. In their model, the spray–wall interaction depends on the film thickness, on the impinging droplet velocity and diameter and on liquid density, viscosity and surface tension. Lee et al. (2000, 2001) showed that some of the previous discussed models significantly underestimate the height of the splashed cloud. Accordingly, they suggested to include a static model of the wall film.

In previous papers the models by O'Rourke and Amsden (1996, 2000), by Bai and Gosman (1995) and by Lee et al. (2000, 2001) have been compared in terms of performance and capability of representing the splash phenomenon (Allocca et al., 2006a,b; Andreassi and Ubertini, 2005). The three models behave similarly at low injection pressure (from 15 to 30 MPa) and ambient back-pressure. However, the model by Lee et al. (2000, 2001) shows the best agreement with the experimental data provided by Katsura et al. (1989), Saito et al. (1993) and Fujimoto et al. (1990). Under high injection pressures (120 MPa and 80 MPa), typical of modern DI Diesel engines, all the three models in their original version proved to be inadequate to correctly reproduce the splash phenomena, but the model by Lee et al. (2000, 2001) still resulted to be the best performing (Allocca et al., 2006a,b).

This paper reports an experimental study on the impingement of a diesel spray onto a flat surface at different operating conditions and presents a new splash model by modifying the empirical correlations used by Lee et al. (2000, 2001) on the basis the experimental results.

The paper is organized as follows. First, the main features of the splash model proposed by Lee et al. (2000, 2001) are discussed and the model capabilities are tested comparing the numerical results with the experimental data provided by Katsura et al. (1989), Saito et al. (1993) and Fujimoto et al. (1990). Then, after the description of the experimental facilities and techniques, the experimental spray–wall interaction for a spray injected by a Common Rail (CR) injection apparatus in a constant volume vessel is shown for two different injection pressures, 800 and 1200 bar with a back-pressure ranging between 0.1 and 5 MPa. The dependence of the secondary spray properties on wall temperature is also discussed. Finally, a general enhanced formulation of the splash model proposed by Lee et al. (2000, 2001) is provided and is validated in terms of splash height and radius at different injection and chamber pressures.

2. Multi-dimensional numerical tool

The splash model is implemented in a modified version of the KIVA-3V code that solves the three-dimensional equations of chemically reactive flows with sprays with a multi-block structured grid approach. Although a detailed description of several of the implemented submodels can be found in previous papers (Andreassi and Ubertini, 2005; Allocca et al., 2006a,b; Bella et al., 2002; Ubertini et al., 2004), before describing the data analysis performed with the numerical simulation tool, it is appropriate to briefly highlight the main features of the submodels related to the spray formation.

2.1. Atomization

The atomization mechanism is simulated through a hybrid approach, which distinguishes between a jet primary breakup and a droplet secondary breakup. Primary break-up consists in the atomization process that may take place inside the injector to the dense part of the spray. Secondary break-up describes how the parcels of liquid initially formed are transformed to a dilute spray, composed of small spherical droplets.

Due to the high speed of the flow inside the injection nozzle in modern CR systems, the small size of the exhaust orifices and the high pressure, the jet surface at the nozzle exit is already disturbed or even atomized. Above a certain injection pressure, which depends on the nozzle geometry and on the in-cylinder pressure, cavitation appears at the sharp inlet corner of the nozzle and eventually reaches the nozzle exit. Accordingly the primary breakup inside or immediately after the nozzle orifices is produced (Bella et al., 1999; Chaves et al., 1995).

In the primary jet break-up phase a combined approach of turbulence, cavitation and droplet surface wave-like disturbance is used. The phenomenological flow model proposed by Sarre et al. (1999) is used to evaluate the flow regime inside the injector (turbulent or cavitating) and to simulate the effects of nozzle geometry on fuel injection and spray processes. The resulting cavitation predictive submodel provides the initial conditions for the spray model in terms of initial parcels size and velocity.

The related turbulent kinetic energy and its dissipation rate are also evaluated to predict jet atomization due to turbulence as proposed by Hu and Gosman (1991). The possible cavitation effects are considered as a source of turbulent fluctuation inside the spray. The Wave Breakup (WB) model (Reitz and Diwakar, 1987), based on a stability analysis of liquid jets, is also used to simulate primary atomization of liquid core. Each model provides a time-scale of atomization. The time-scale, which produces the fastest set-off of instability, is chosen to set-off the break-up event.

The secondary break-up is a complex flow phenomenon in which inhomogeneous pressure distribution on the surface of the droplet leads to shape deformation and then to droplet breakup. Deformation and breakup of a liquid droplet by aerodynamic forces is classified through the Weber number, which is the ratio between the inertia and the surface tension forces. A critical Weber number ($We_c = 12$) is the limit over which deformation leads to breakup. Depending on the intensity of the aerodynamic force, five distinct regimes are considered: vibrational, bag, chaotic, stripping and catastrophic (Bella et al., 2002). Each of these regimes is assumed to exist in a certain range of the Weber number and for each regime a distinct secondary breakup model is called by the code for estimation of secondary droplets atomization: the standard Taylor Analogy Breakup (TAB) model (O'Rourke and Amsden, 1987) for the vibrational regime (slower droplets, usually at the periphery of the spray); the Droplet Deformation and Breakup (DDB) approach (Ibrahim et al., 1993) for the bag breakup; the WB model for the stripping regime (Reitz and Diwakar, 1987); a competition between the DDB model and the WB model for the chaotic regime; a competition between the R–T model (Patterson and Reitz, 1998) and the WB model for the catastrophic regime. Finally, the collision and the coalescence models of the original version of KIVA-3V are considered (O'Rourke and Amsden, 1987).

2.2. Splash modelling

Spray wall interaction is influenced by many physical and kinematics parameters, which can be summarized as follows:

- fuel density, ρ: the impinging pressure over the contact surface is proportional to the liquid density;
- fuel surface tension, σ: the resistance force to droplet deformation is proportional to the surface tension;
- fuel viscosity, μ: high droplet viscosity enhances the energy consumption during the spreading stage and also contributes to delay secondary disintegration upon impingement;
- impinging droplet size, d_i: the impact kinetic energy is proportional to the droplet volume and then to the droplet diameter; furthermore, droplet size exerts a direct influence on the deformation and film spreading on the surface upon its collision because the impact pressure peak decreases with the drop size;
- impinging droplet velocity, $\vec{V}_i$: deformation and radial flow of the impinging droplet are determined directly by the droplet velocity, as the impact pressure acting on the impinging droplet surface is approximately $\rho w_0^2/2$, being w_0 the normal velocity before impingement; the impinging velocity is directly related to the injection pressure, p_{inj} and the back-pressure, p_{ch};
- wall temperature, T_w: the energy exchange close to the wall is driven by the wall temperature and, as a consequence, the droplet can evaporate or condensate;
- droplet impact angle, α: the mass exchange between the impinging droplet and the film depends on the impact angle;
- depth of liquid film covering wall surface;
- near wall gas boundary layer;
- wall roughness.

Usually the impact and the evolution of a spray are described in terms of dimensionless numbers that summarise the cited characteristics: Reynolds (Re), Weber (We), Laplace (La) and Ohnesorge (Oh).

Although detailed multi-phase CFD modelling of the spray–wall interaction could be preformed, its computational costs make it unsuitable to be coupled with a detailed internal combustion engine multi-dimensional simulation. Therefore, simplified phenomenological models are required, because of their effectiveness in providing accurate information while maintaining acceptable computational times.

Basically, two main issues need to be addressed in modelling spray impingement. The first is to establish a set of transition criteria to predict which regime occurs. The second is to quantitatively estimate post-impingement characteristics such as rebound velocity, fraction of the mass deposited on the wall, size and velocity distributions of the secondary droplets for the splash regime. Different impingement regimes are identified for dry and wetted surfaces depending on the impinging droplet Weber number (We) (or kinetic energy) and the wall conditions (Bai and Gosman, 1995):

- stick, when the droplet forms liquid film and adheres to the surface in a nearly spherical form;
- rebound, when the droplet hits the wall at low impact energy and bounce back;
- spread, when the droplet forms liquid film and, being its impact energy high enough, merges with the liquid film;
- splash, when each droplet generates some secondary parcels and film.

Considering that in modern Diesel engines the velocity of impinging droplets is usually very high, the present analysis is focused on the splash regime, which is the most frequent occurring one. Among the models available in literature, the model proposed by Lee et al. (2000, 2001) (from now on called LR model) has been selected because of its performance and capability of representing the splash phenomenon, with particular emphasis on Diesel sprays. The proposed model accounts for mass and energy conservation and features empirical correlations for the unknown quantities.

The regime transition criterion used for predicting if splashing occurs is quantitative determined by means of the impinging droplet Weber (We_0) and Reynolds (Re_0) numbers as proposed by Mundo et al. (1995):

$$E = We_0 Re_0^{0.25} > 57.7, \tag{1}$$

where E is a dimensionless impact energy parameter.

As experimentally demonstrated by Roisman and Tropea (2005), upon impact of a high velocity droplet on a flat wall, a fluctuating liquid layer is formed with the creation of an expanding crown-like sheet. The unstable liquid surface of the peripheral crown is followed by the formation of a number of uprising jets which then break up into many secondary droplets, also called satellite or splashed droplets. Therefore, the description of the splash phenomenon is complex and necessarily requires calculating many post-impingement quantities, mainly the secondary droplets size, mass and velocity and the portion of the incident mass and momentum transmitted to the liquid film. Fig. 1 shows a schematic diagram of impinging and splashed droplets, highlighting the main kinematics parameters calculated by the model and the coordinate system.

The total splashed mass is determined by means of the impinging mass, under the hypothesis made by Bai and Gosman (1995) that, for a spray impinging on a wetted surface, the splashed mass may be even greater than the impinging mass since the secondary droplets may take some liquid out from the film. The ratio of the splashed mass to the incident mass, r_m, is calculated as

$$r_m = \frac{m_s}{m_i} = A + \mathrm{Random}(0, B), \tag{2}$$

where $A = 0.2$ and B corresponds to 0.6 for a dry wall and 0.9 for a wetted wall.

An empirical correlation based on the experimental data of Naber and Farrel (1993) is used to calculate the number of splashed droplets per incident droplet:

$$n_s = 0.187 \cdot We_{0,n} - 4.45, \tag{3}$$

where $We_{0,n}$ is the Weber number of the impinging droplet based on its velocity component normal to the wall.

Once the number of ejected droplets is known, the application of the mass conservation principle allows to determine the secondary droplets size as follows:

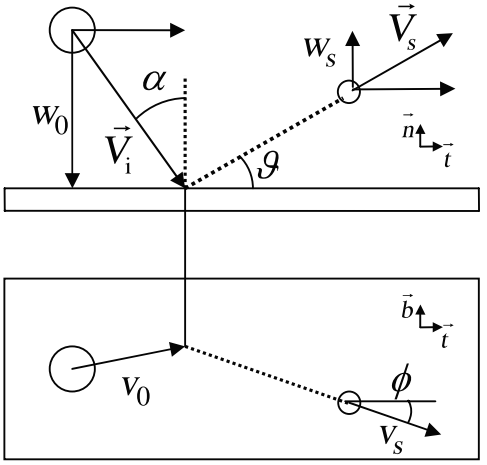

Fig. 1. Schematic diagram of impinging and splashed droplets.

$$d_s = \left(\frac{r_m}{n_s}\right)^{1/3} d_i. \tag{4}$$

The determination of the splashed droplets velocity components is the element that mainly characterizes the different models available in literature. Lee et al. (2000, 2001) calculate the splashed droplet velocity magnitude applying the energy conservation law and using the experimental observations made by Yarin and Weiss (1995). This results into the following expression of the splashed droplet Weber number:

$$We_s = \left(\frac{r_m}{n_s}\right)^{1/3} \frac{1}{r_m}\left[We_0 - \left(72\frac{We_{0,n}}{Re_0} - 12\right)\right] - 12, \tag{5a}$$

$$|\vec{V}_s| = \left(\frac{\sigma \cdot We_s}{\rho \cdot d_s}\right)^{0.5}, \tag{5b}$$

where $\vec{V}_s$ is the velocity vector of the splashed droplets.

The tangential component of the splashed droplets velocity is calculated starting from the tangential velocity of the liquid crown given by the theoretical relationship of Yarin and Weiss (1995):

$$v_s = \frac{0.452 \cdot K_f \cdot Re_{0,n}^{1/8} \cdot w_0}{\sqrt{\Psi}}, \tag{6}$$

where $\psi = 1$ for $Re_{0,n} \leqslant 577$ and $\psi = 0.204 Re_{0,n}^{0.25}$ elsewhere.

The term $\vec{V}_s$ can then be determined after the azimuthal angle, ϕ, is calculated by means of the correlation proposed by Naber and Reitz (1988).

2.3. Film modelling

The wall film model employed in the present simulations derives from the research of O'Rourke and Amsden (1996). This model is able to represent the wall film dynamics keeping into account all the major physical processes affecting the liquid film including mass, momentum and energy contribution to the film due to spray impingement, splashing effects, shear forces, heat transfer in and above the boundary layer, etc.

The major assumption of the model is that the fuel film is so thin that the film flow is laminar and that the inertial force can be neglected. This assumption is no longer valid in the vicinity of sharp corners where an inertial separation criterion is considered.

A particle numerical model is used for the wall film for the compatibility with the spray model and for the possibility to easily calculate the film convective transport.

3. Spray simulation results: comparison with literature experimental data

The numerical results obtained through the previously described model for spray impingement were compared to the measurements performed by Katsura et al. (1989), Saito et al. (1993) and Fujimoto et al. (1990). The experimental conditions are reported in Table 1. The fuel spray emerges from a single hole nozzle and impinges upon a wall at a distance of 24 mm from the tip of the injector for tests 1, 3 and 4, and of 34 mm for test 2. The injection pressure, p_{inj}, is 14 MPa for tests 1 and 2, 13.8 MPa for test 3 and 30 MPa for test 4. Diesel with density 822 kg/m^3 and kinematics viscosity 2.6 mm^2/s is used as the working fluid.

The computational domains used for the simulations are a $50 \times 50 \times 40$ mm^3 grid for the test cases 1, 3 and 4 and a $50 \times 50 \times 45$ mm^3 grid for the test case 2, with a 0.75 mm spacing, which was found to be fine enough to reduce the grid-size sensitivity of less than 1% in terms of spray penetration. The maximum time-step was set to 0.01 ms in order to fix the maximum number of injected droplets per time-step and the code automatically reduces the time-step if required by convergence restrictions. A total of 4000 sample parcels are introduced throughout the injection duration time.

Fig. 2 shows the comparison between experimental and numerical splash height as a function of time. The criteria for determining the splash height is the 95% accumulated splashed mass distance from the wall.

Despite the differences of the test conditions, the first three cases give similar results in terms of splash height, highlighting how the most affecting parameter is the injection pressure. In all these tests a good agreement is observed with a slight overestimation of the final splash height.

Under the conditions of the Test #4, with an injection pressure higher than the previous three cases, the numerical splash height is lower than the experimental one. This opposite trend is probably related to the experimental correlations used in the model which often refer to a single droplet behaviour with low impinging velocity or to a low injection pressure spray. This preliminary analysis suggests to further stress the model capabilities investigation by studying the model performances under the actual Diesel injection pressures.

It is worth mentioning that also in test case #1, even observing a final numerical value slightly over the experimental one, the predicted splash height is below the measured one for most of the observed range. Considering that the only difference with test case #2 is the nozzle distance from the wall, this can be still related to the change in the impinging droplets velocity and then Weber number.

4. Experimental apparatus

An experimental apparatus properly devoted to investigate the high pressure sprays interactions with walls has been realized. In the next sections the main components will be described in detail. A schematic diagram of the experimental apparatus is reported in Fig. 3a.

Table 1
Specification of test conditions

	Test 1: Katsura et al. (1989)	Test 2: Katsura et al. (1989)	Test 3: Fujimoto et al. (1990)	Test 4: Saito et al. (1993)
Injection nozzle	Single hole	Single hole	Single hole	Single hole
Nozzle diameter [mm]	0.3	0.3	0.2	0.25
Nozzle length [mm]	2.0	2.0	2.0	2.0
Injection pressure [MPa]	14	14	13.8	30
Fuel injection duration [ms]	1.2	1.2	1.3	2.85
Injected fuel mass [mm^3]	10.5	10.5	8.3	35
Back-pressure [MPa]	1.5	1.5	1.5	2.1
Distance from the wall [mm]	24	34	24	24
Gas temperature [K]	293	293	293	293
Injection angle [°]	0	0	0	0

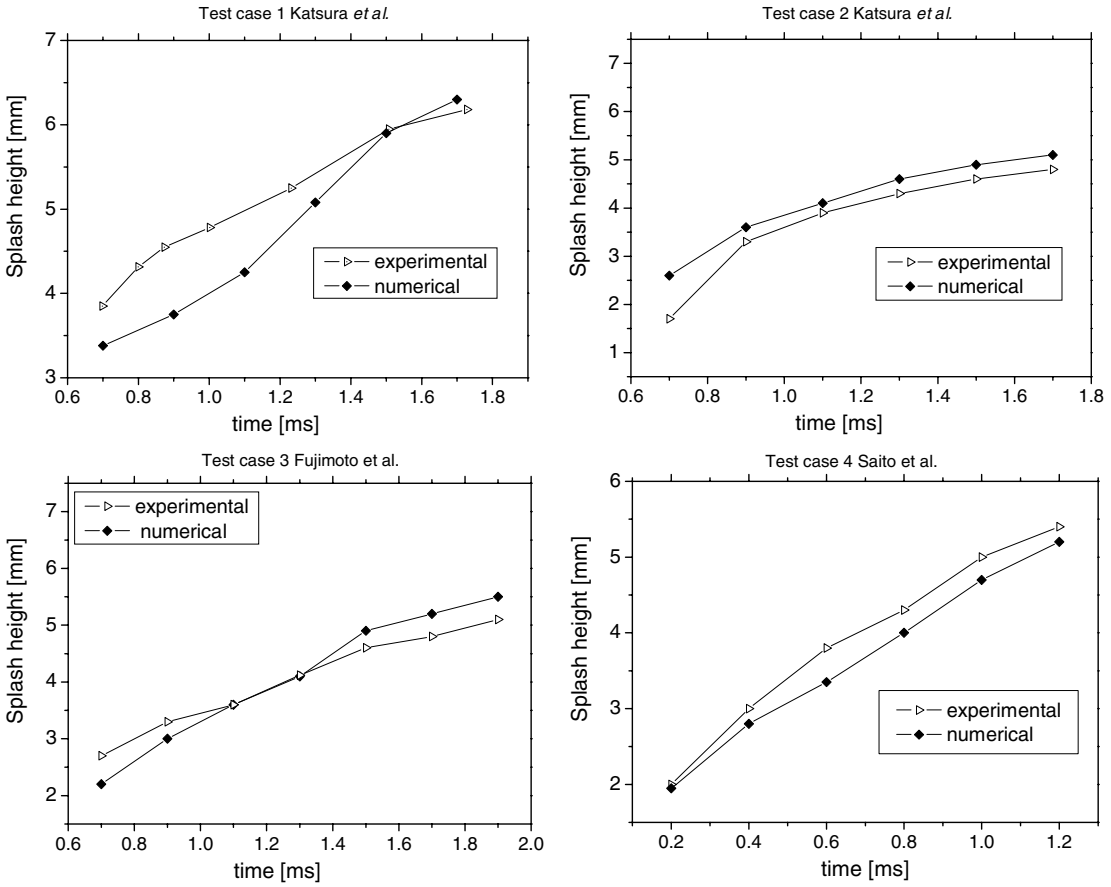

Fig. 2. Comparison between numerical and experimental literature splash height under low injection pressure (splash height is the 95% accumulated splashed mass distance from the wall).

4.1. High pressure vessel

The Diesel spray evolution and fuel-wall impingement are investigated in an optically-accessible high-pressure vessel (Fig. 3b) equipped with three large quartz windows (80 mm). Two windows are aligned for the spray lightning while a third one is located at right angle for collecting the scattered light. The injector is placed on the top of the vessel spraying the fuel along the quartz windows diameter. The inner diameter of the chamber is 125 mm and the total volume of the bomb is 8 dm^3 allowing both free spray evolution and wall impingement analyses. The chamber has been filled with nitrogen (N_2) at pressures up to 5.0 MPa measured by an inner located pressure transducer with an uncertainty of 0.01 MPa.

A stainless-steel flat-plate is introduced in the pressure vessel and an x–z–φ micrometric apparatus is used for its translation and tilting with respect to the jet axis. For the present analysis, the plate is placed 22 mm (±0.1 mm) from the nozzle at right angle with respect to the spray axis. A 200 W electrical resistance heater allows plate heating up to 500 °C and temperature is controlled by a Watlow 985 Series system (±1 °C) using a J-type thermocouple located at the centre of the plate 0.5 mm under the impinging surface. Also, the chamber gas temperature is monitored by a thermocouple. In this paper the wall temperature ranges between 20 and 500 °C and the back-pressure between 0.1 and 5.0 MPa in N_2 non-reactive gas.

4.2. Injection system and fuel gauge meter

The sprays are generated in single-shot mode by a common rail injection system. Open software allows setting injection pressure, injection duration and timing via a Programmable Electronic Control Unit (PECU).

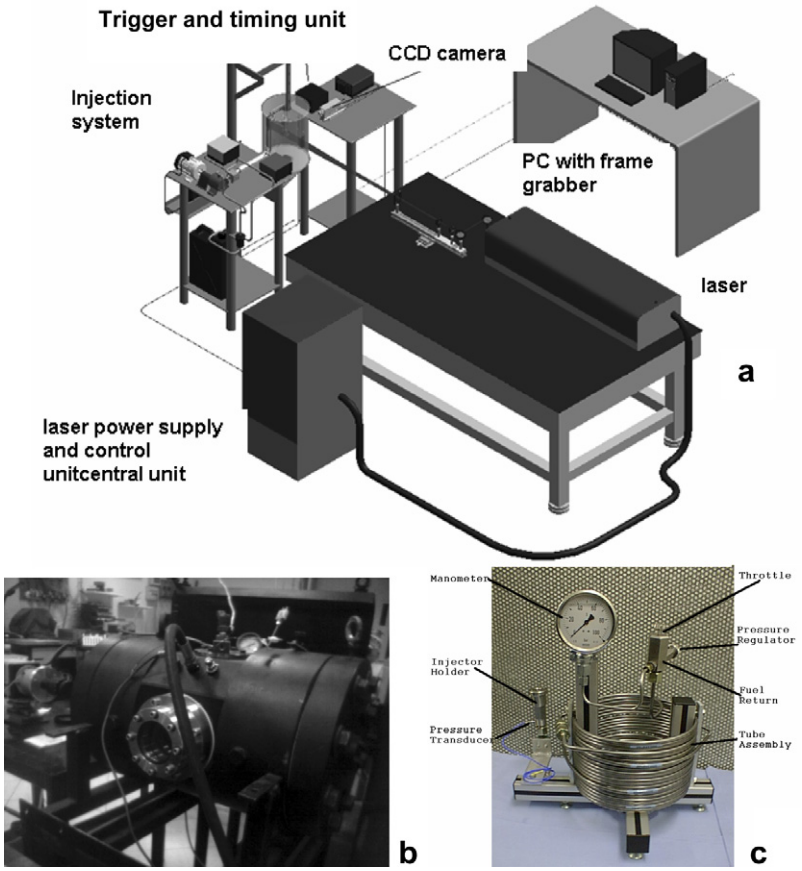

Fig. 3. Schematic diagram of the experimental apparatus (a) and digital photo of the high pressure vessel (b) and of the AVL fuel injection meter (c).

Injection pressures of 80 and 120 MPa are set with a nominal injection duration of 1.0 ms. The ISO 4113 (1998) calibration fluid is used. An axial single-hole nozzle with hole diameter and length of 0.18 and 1.0 mm, respectively, is employed. An AVL Fuel Injection Meter (Fig. 3c) measures the instantaneous fuel injected quantities with a time resolution of 5 μs (Allocca et al., 2003), thus allowing the knowledge of the amount of the delivered fuel at the time correspondent to the captured frame and to relate it to the scattered light intensity. An example of the fuel injection rate signal is reported in Fig. 4 for a single strategy, 1.0 ms nominal duration and 120 MPa injection pressure. The effective injection duration is 1.6 ms with a total delivered fuel of 7.99 mg.

4.3. Image acquisition

A laser sheet is derived from the second harmonic of a Nd-YAG pulsed laser (532 nm) with a thickness of 100 μm and a height of 50 mm. The spray, developing along the diameter of the chamber and the line of sight of the quartz windows, is lightened by the laser sheet along its axis for the non-impacting spray and along the diameter of the annular zone for the impacted fuel. The scattered light is collected at right angle by a synchronized CCD camera. An injector/laser/CCD electronic control configuration allows collecting images at different instants from the Start Of Injection (SOI). The frames are captured by a PULNIX TMC-6 CCD camera 768×568 pixels, 8 bit resolution. With the realized configuration, the resulting spatial resolution is 11.1 pixels/mm, 8.0 pixels/mm and 7.8 pixels/mm at 1, 3 and 5 MPa of back-pressure, respectively, with focal length optic of 28 mm.

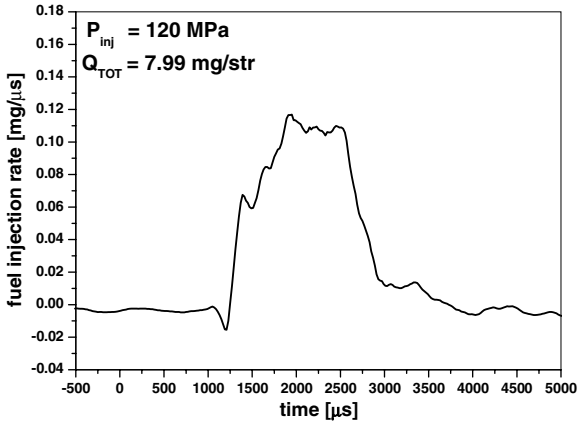

Fig. 4. Fuel injection rate profile (single strategy, 1.0 ms nominal duration, 120 MPa injection pressure, effective injection duration 1.6 ms, total delivered fuel 7.99 mg).

A Digital Delay & Pulse Generator by Stanford Research System Inc. and a Tektronix TDS 684 B (1 GHz) Four Channel Digital Scope synchronize, delay and control the laser/detector system with respect to TTL pulse command with a high temporal resolution. Further details of the apparatus are reported in (Allocca et al., 2002).

Spray structure and morphology, jet cone angles, tip penetrations and impact geometry are measured by professional software developed for processing the acquired images.

5. Experimental results and discussion

5.1. Image processing and procedures

The images of the spray impacting on the flat wall need to be post-processed for the extraction of the parameters of interest. The impinging spray can be characterized both in terms of fuel geometry and fuel density distribution. It is worthwhile depicting the fuel contour for collecting the geometrical parameters (radial growth, leading edge, thickness) and grouping the scattered light intensity to highlight different density zones.

Most of the images are affected by background noise related to light scattering of residual floating droplets and dust in the vessel and overexposures in high fuel density zones and finely atomized non-impacting droplets. The last effect is particularly significant in the free evolving zone (before the impact on the wall) where, due to the high velocity of the emerging droplets, a strong interaction with the surrounding gas and stripping of ligaments from the spray body occurs.

The acquired image is first converted in a 256 grey levels scale from the initial RGB acquisition mode. A restricted dilation function from the image processing software (Image Pro Plus) is applied for background subtraction and stray light reduction while a contour enhancement has been obtained by a suitable 3×3 median filter.

Fig. 5 shows the results of the digital image processing at $p_{inj} = 80$ MPa, $T_{wall} = 298$ K and $p_{ch} = 0.1$ MPa. In the upper part of the figure, the acquired spray at 200 μs from the SOI is reported (left side) while in the right part the image after the digital processing is shown. In the low part analogues images are reported at 1100 μs from the SOI. It is worth noting that the background diffused light in the frame and the overexposure due to the finely atomized light around the jet evolution are suppressed without significantly affecting the spray geometry. An evaluation of the suppressed fuel, based on the scattered light intensity, returns values around 98–99%. The jets contour at early (200 μs) and late (1100 μs) impact are clear and they preserve the outline dynamic characteristics of the impinging spray evolution, thus making clearly evident the light intensity distribution.

In Fig. 6, a pseudo-colour image grouped as iso-intensity is reported for an 80 MPa injection pressure spray impacting at 1200 μs from the SOI at atmospheric back-pressure and plate ambient temperature. Five iso-intensity groups are identified.

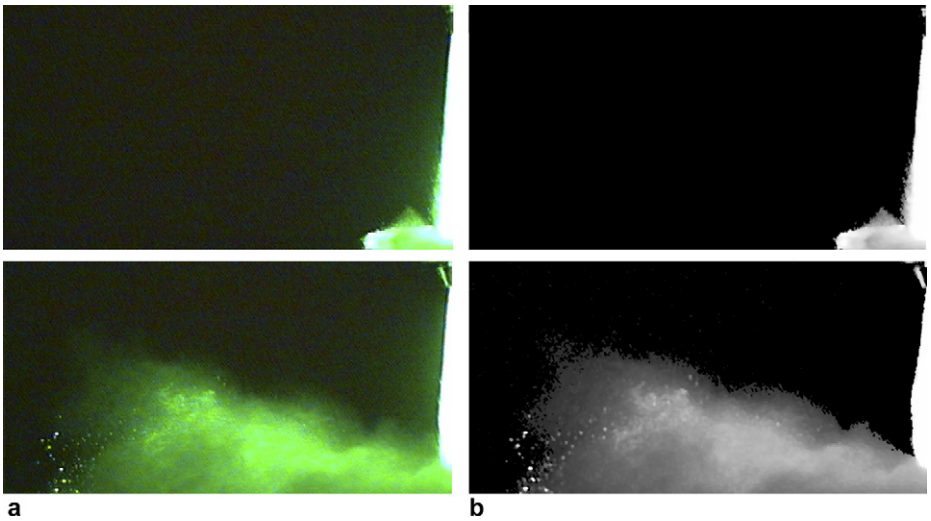

Fig. 5. Digital image processing of impacting spray, at $p_{inj} = 80$ MPa, $T_w = 298$ K and $p_{ch} = 0.1$ MPa, at 200 μs (upper row) and 1100 μs after SOI (lower row). (a) non-processed images and (b) processed images.

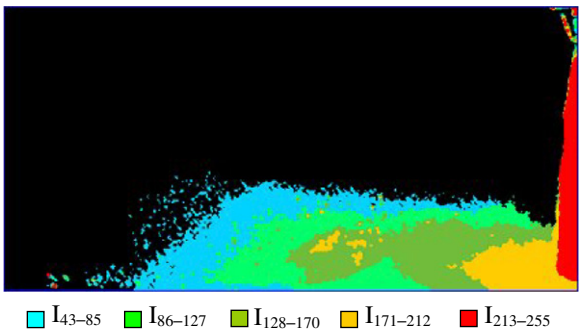

Fig. 6. Image in pseudocolor of impacting spray with scattered light iso-intensity zones.

The volumes of the different iso-intensity regions, V_i, are calculated making the hypothesis of a spatial uniform distribution of the fuel with respect to the spray axis and applying the Pappo's theorem.

The working procedure is a baseline hypothesis and it is normalized to the total amount of the injected fuel (measured by the fuel injection rate system):

$$\frac{1}{n} V(t) \sum_{i}^{n} \rho_i(t) = m(t) \tag{7}$$

being n the number of groups, ρ_i the fuel density in the group (i), $m(t)$ the total fuel injected mass and $V(t)$ the volume occupied by the spray at the instant t.

Under the hypotheses that the fuel spray is fully atomised into droplets in the splash region and that the light intensity scattered by the droplets is proportional to their particle concentration, a relationship between the light intensity and particle concentration can be obtained. As a confirmation, it is possible to note as the highest value is placed in the non-impacting zone, which is the dense spray zone, while lower values are observed in the periphery of the rebounded spray, partially on the crest and mostly in the outer side indicating a higher penetration of the surrounding gas in the jet.

Moreover, assuming that the secondary droplets are all of the same size, the particle concentration can be related to the fuel density.

Table 2
Calculated values of coefficient a

Time [μs]	Calculated coefficient a [10^{-6}mg/mm^3]	Deviation (%)
250	1.19	7.2
300	1.17	5.4
500	1.01	9.0
700	1.09	1.8
1000	0.99	10.8
1200	1.21	9.0
Mean value	1.11	

Table 3
Mass distribution at 300 μs

Grey levels	Mass distribution
43–85	ρ_{43-85} (=0.08 kg/m^3)
86–127	1.5 ρ_{43-85}
128–170	2.0 ρ_{43-85}
171–212	2.6 ρ_{43-85}

The previous assumptions may be acceptable if the objective is to obtain a relative trend of the fuel density distribution and without putting forward a claim on the exact values. However, nothing can be said on the density distribution in the jet core region (grey levels from 213 to 255) where the spray is dense and the particle size distribution is extremely varied.

The following procedure is defined and performed in order to demonstrate that in each zone (see Fig. 6), with the exception of the jet core, the resulting average fuel density is proportional to the average light intensity and to quantify the fuel distribution in the splash region:

- calculation of the 5 volumes at time t_i of the ith frame;
- calculation of the 5 average intensities at time t_i of the ith frame;
- calculation of the instantaneous splashed mass flow rate $m(t)$ from the injection profile of Fig. 1 and the knowledge of the fuel mass within the jet core $m(t)_{213-255}$ (grey levels 213–255). Definition of the relationship among mass flow rate, volumes, V, average light intensities, I, and an unknown coefficient, a

$$m(t) - m(t)_{213-255} = a \cdot (\overline{I}_{43-85} \cdot V_{43-85} + \overline{I}_{86-127} \cdot V_{86-127} + \overline{I}_{128-170} \cdot V_{128-170} + \overline{I}_{171-212} \cdot V_{171-212}), \quad (8)$$

  where the subscript refer to the grey levels range;
- calculation of the unknown coefficient a for different times;
- verification that the coefficient a is constant within the time and definition of the proportionality between light intensity and particles concentration;
- calculation of the mass distribution among the different zones.

Table 2 reports the results of this procedure, demonstrating that the coefficient a is constant with time with a maximum deviation of 10%. As an example at $t_i = 300$ μs from the SOI, Table 3 reports the evaluation of the mass distribution between the different zones using the previous defined procedure.

6. Experimental results and discussion

The spray–wall impingement may be well characterised by reporting both the geometry of the fuel distribution on the plate versus injection and ambient conditions and the density distribution to evaluate the local air–fuel ratio. In this paper two injection pressures, 80 and 120 MPa, and four back-pressures, 0.1, 1.0, 3.0 and 5.0 MPa, are considered, covering typical diesel gas density in the combustion chamber in all operative

conditions. The fuel impacts on the plate at a temperature ranging from 20 °C to 500 °C, for atmospheric back-pressure, and to 300 °C for back-pressure up to 5.0 MPa.

Characteristic parameters of the impact are the radial growth (r_g) of the fuel on the plate meaning the maximum elongation of significant droplets far from the spray axis and normally to it and the maximum thickness (t_h) of the splash cloud generated by the secondary droplets, as shown in Fig. 6.

6.1. Spray impingement geometry

In Fig. 7 the radial growth (r_g) of the impacted fuel is reported versus time from the SOI for 80 MPa (left) and 120 MPa (right) injection pressures being the back-pressure equal to 1.0 MPa. The investigated plate temperatures are 23, 100, 200 and 300 °C. At 80 MPa the radial growth of the fuel on the plate increases almost linearly in time and the displacement from the spray axis is monotonic with respect to the growing temperatures. The heat transfer effect on the radial growth is immediately evident at low temperatures (between ambient to 100 °C) while, at higher values, the effect is still evident but reduced in magnitude.

In the right hand side of Fig. 7 the radial growth r_g for an injection pressure of 120 MPa is reported. Despite the breaking in segments and some overlapping of the curves, the trend is quite similar to the lower pressure events: the wall temperature plays an important role. Higher radial penetrations can be measured varying from 35.4 mm, at ambient temperature and 1200 μs from the SOI, to 36.8 mm at 300 °C and 1000 μs. Higher injection pressures imply higher velocities of emerging droplets from the nozzle and higher radial components of secondary droplets velocity forming the hypothesis that the wall-droplets heat exchange is analogues to the case at 80 MPa of injection pressure. Also the different amount of fuel delivered for different injection pressures must be taken into account (i.e. at 1000 μs from the SOI the total injection quantities at 80 and 120 MPa are 3.68 and 4.86 mg, respectively). A more complete reference for the injected quantities and the corresponding times is reported in Table 4.

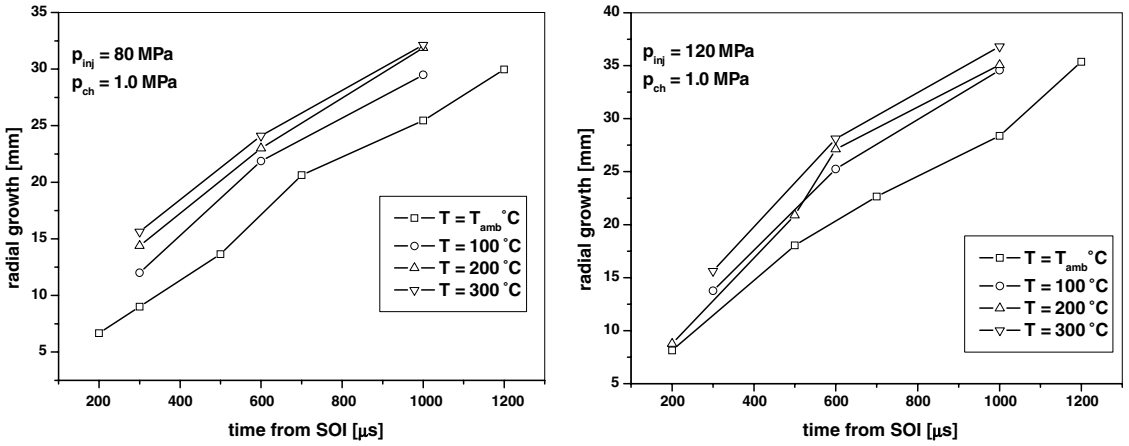

Fig. 7. Radial growth of impacted sprays for different temperatures of the plate (80 MPa (left) and 120 MPa (right) injection pressures being the back-pressure equal to 1.0 MPa).

Table 4
Injected fuel quantities at different time from SOI and injection pressures

Time from SOI [μs]	Inj. quant. [mg] at 80 MPa	Inj. quant. [mg] at 120 MPa
1000	3.68	4.86
1100	4.14	5.42
1500	5.69	7.21

Regarding the fuel thickness on the plate, an introducing consideration is needed. Referring to Fig. 6, the fuel thickness does not assume constant values along the entire radial distance of spread fuel. Fujimoto et al. (1997) report a schematic view which shows an "impingement region" on the plate immediately downstream the nozzle (around the spray axis), followed by a "main wall jet region" with a thin restricted vena of the

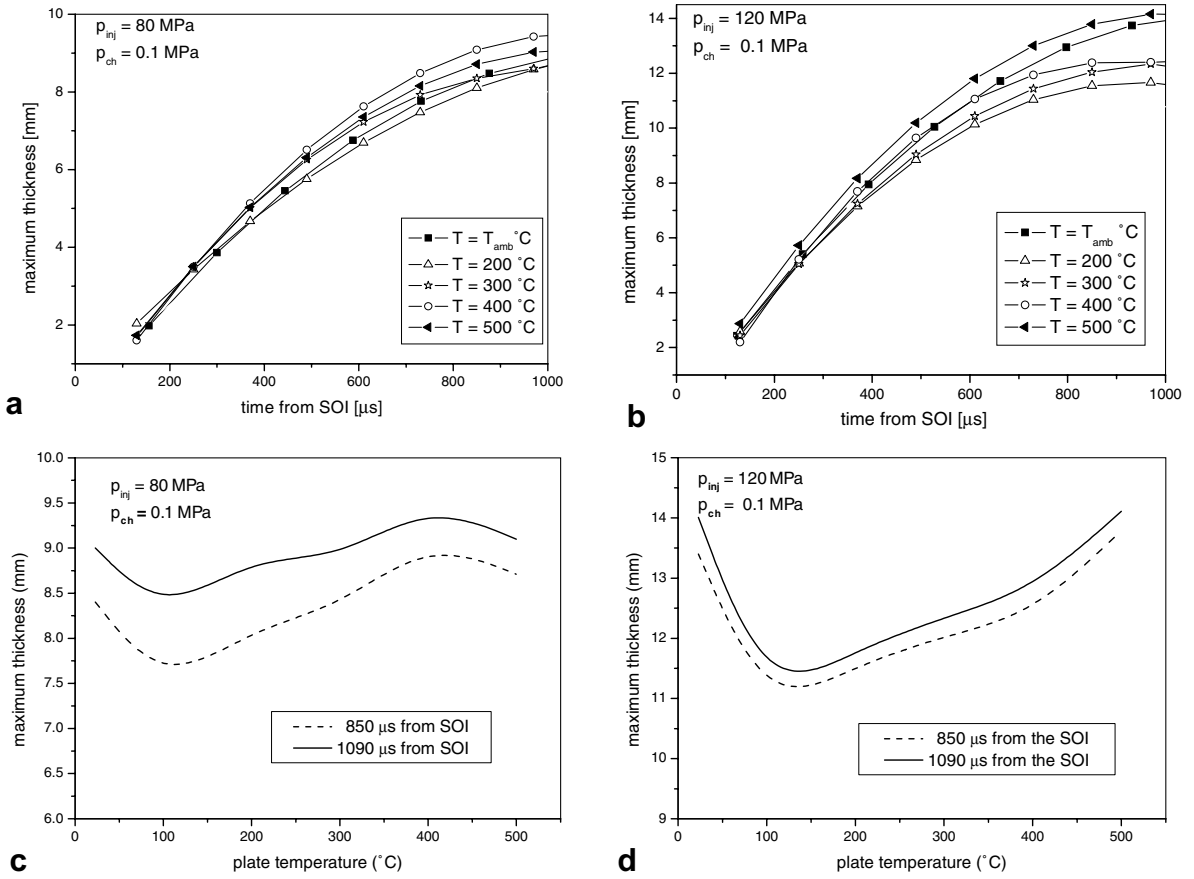

Fig. 8. Maximum thickness of impacted sprays for different temperatures of the plate.

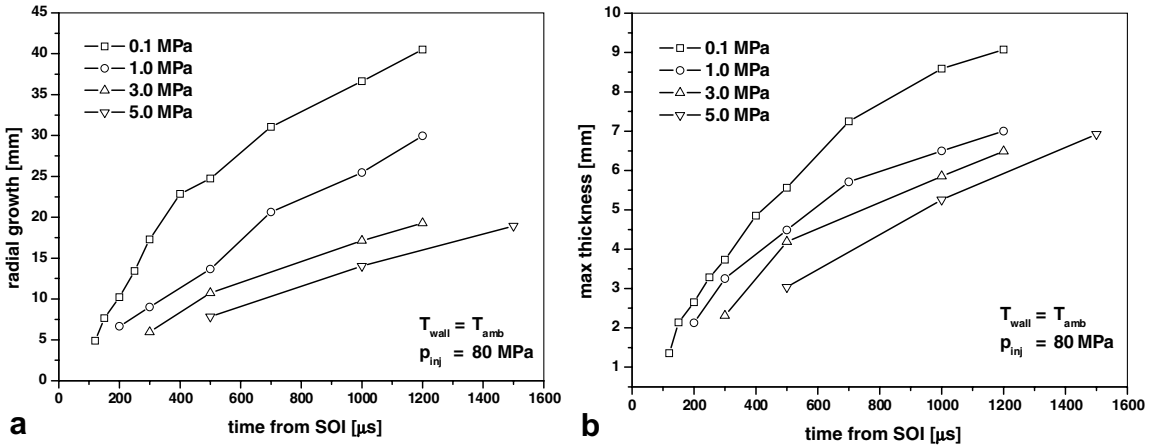

Fig. 9. Effects of the vessel gas pressure on radial growth (a) and maximum thickness (b).

rebounding fuel and, finally, a "wall jet vortex region" where an inversion of droplets tangential speed occurs characterized by a maximum thickness of the film on the plate. In Fig. 8a and b maximum thickness measurements of the spread fuel versus time after the SOI are reported for 80 MPa (left) and 120 MPa (right) of injection pressure being the back-pressure equal to 0.1 MPa in both cases. The effects of the fuel injection pressure and the wall temperature on t_h are quite similar to those on r_g, even if some particular trends can be observed, as highlighted by the graphs of Fig. 8c and d where the maximum thickness is plotted versus the plate temperature for two different times from SOI (850 and 1090 μs). This could be probably due to the fact that the resulting thickness is a combination effect of the wall temperature – Nukiyama and Leidenfrost effects (Mills and Fry, 1982) – and the normal component of the secondary droplets. In all the cases of Fig. 9 the maximum thickness t_h has a minimum close to 100 °C while an absolute maximum close to 450 °C is observed only at 80 MPa of injection pressure, while at 120 MPa t_h varies monotonically within the temporal investigated range. This particular behaviour could be related to the higher secondary droplets velocity, being the peak shifted toward longer times. The combined effect of the wall temperature and the droplet velocity could explain the lower slope curves after the minimum value compared with the single droplet configuration where a quasi-discontinuity exists between the Nukiyama and Leidenfrost points.

A final general consideration on the effect of the wall temperature on the rebound velocity parameters is that, in the investigated range, the higher is the temperature the larger are both the radial and the axial components.

Fig. 9 shows the effect of the back-pressure on r_g and t_h, being 298 K the plate temperature and 80 MPa the injection pressure. A vessel gas pressure rise from 0.1 MPa to 1 MPa produces a drastic reduction of the radial growth (Fig. 9a). At 1200 μs after the SOI, r_g falls from about 40 mm, at atmospheric back-pressure, to about 30 mm, at 1 MPa and further diminishes down to 19 mm, at 3.0 MPa and 16 mm at 5.0 MPa. Taking as a reference the radial growth at atmospheric back-pressure, reductions of about 40%, 50% and 60% for back pressures of 1 MPa, 3 MPa and 5 MPa, respectively, are observed. Analogous behaviour is observed for the maximum thicknesses in the same operative conditions, as shown in Fig. 9b. It is quite evident that this is a consequence of the rise of the drag acting on the secondary droplets due to the higher pressure in the chamber.

This result is confirmed by the inner fuel density zone identifying where areas at lower density and smallest floating parcels, mainly located at the outline of the splashing jet, reduce at increasing gas pressure (Fig. 10). A compression of the rebound dynamic with a reduction of both the tangential and the normal components of the secondary droplets velocity are observed. A significant consequence in a diesel engine would be a reduced capacity of gas entrainment in the fuel with worst effects on the air–fuel mixing process.

Fig. 11a shows the total volume occupied by the spray at different injection pressures and back-pressures. Passing from 80 MPa to 120 MPa of injection pressure, an injected mass increase of about 30% corresponds to an almost doubled total volume.

At the highest back-pressure (5.0 MPa) and at 1500 μs after the SoI, to a total spray volume rise from 6.3×10^3 mm^3 to 8.5×10^3 mm^3 (~20%) corresponds a total injected mass increase of about 27% (from 5.69 to 7.21 mg). This confirms the significant effect of the back-pressure on the global structure of the spray impacting on the wall.

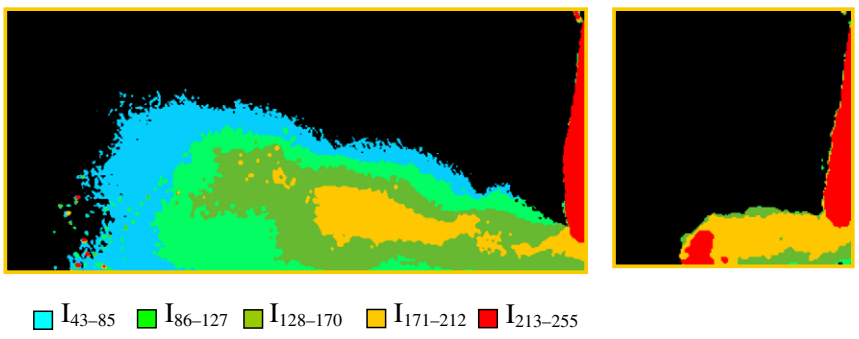

Fig. 10. Effects of the vessel gas pressure (images in pseudocolor) ($p_{inj} = 120$ MPa, $p_{ch} = 0.1$ MPa – left, $p_{ch} = 5$ MPa.

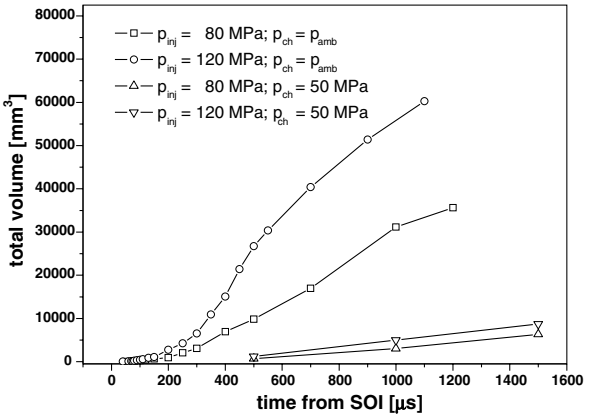

Fig. 11. Effects of injection pressures and back-pressures on the fuel + gas volume.

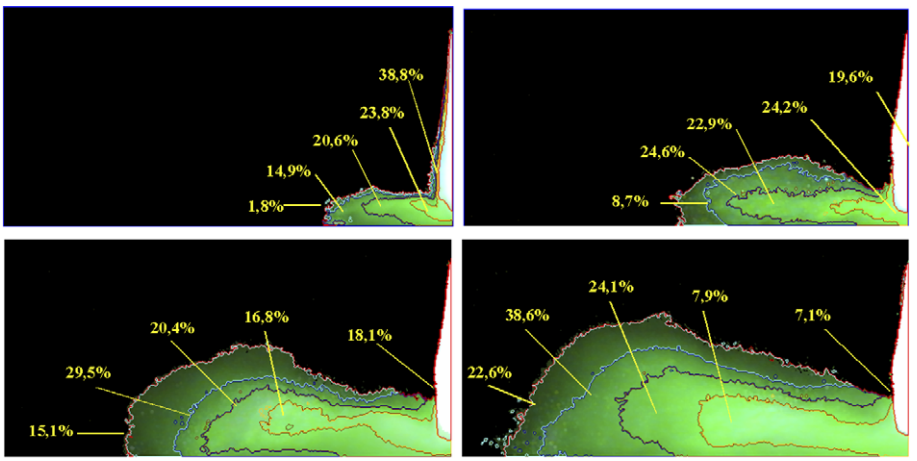

Fig. 12. Time evolution (300 μs, 500 μs, 700 μs, 1200 μs) of fuel iso-density areas of impacting spray injected at 80 MPa on a plate at 298 K and atmospheric back-pressure.

6.2. Fuel density evaluation

The correlation between the full range of scattered light and the fuel density described in the "Image Processing Procedure" section has been applied to the impinging jet images at different times after the SOI.

Fig. 13 reports the time evolution of the iso-density zones for 80 MPa of injection pressure, atmospheric back-pressure and plate at ambient temperature. At 300 μs from the SOI about 40% of the injected fuel is confined in the highest density group ($\rho_{213–255}$). The nearest less dense region ($\rho_{171–212}$) contains about 24% of the total fuel mass and includes the first rebounding secondary droplets. 20.6% and 14.9% of fuel mass are confined in the following two zones ($\rho_{128–170}$ and $\rho_{86–127}$) and only 1.8% is assigned to the less dense group ($\rho_{43–85}$), which is confined in the contour part of the impact, as indicated in the top/left of the Fig. 9. At 500 μs from the SOI (top/right) the amount of fuel confined in $\rho_{213–255}$ zone drastically reduces (19.6%) while $\rho_{171–212}$ remains quite constant (24.2%). The fuel mass present in the intermediate regions ($\rho_{128–170}$ and $\rho_{86–127}$) increases to about 23–24% and that in the last less dense region, $\rho_{43–85}$ jumps to about 9%. As time increases (700 and 1200 μs) a further decreasing of the fuel mass in the highest density regions and a correspondent increase of that in the less dense groups is observed, as at 1200 μs about 60% of the total mass is confined in the splash cloud periphery (22.6 % in $\rho_{43–85}$ and 38.6% in $\rho_{86–127}$). It is interesting to note that the $\rho_{171–212}$ group, the

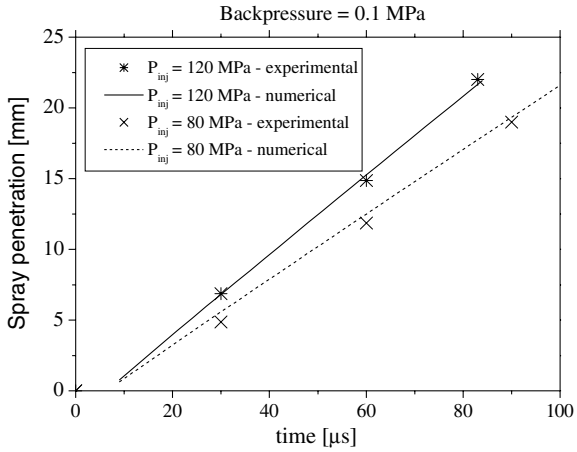

Fig. 13. Spray penetration: numerical–experimental comparison at different injection pressures.

nearest impingement region, is never in contact with the wall indicating a high density of secondary droplets with a strong axial component of velocity.

7. Numerical results and splash model validation

The test cases used to validate the spray–wall interaction submodel, as well as most of the test cases found in literature, are characterised by low injection pressure and they are not representative of the injection conditions in modern DI Diesel engines. Accordingly, in this section the numerical results are compared with the experimental data found under Diesel-like injection pressures and discussed in the previous sections, in terms of secondary droplets cloud shape. Two different injection pressures are investigated (80 MPa and 120 MPa) with a back-pressure ranging from 0.1 to 5 MPa. Considering that the aim of the present study is the development of a reliable phenomenological model of the spray impingement phenomenon with high impact velocity, the analysis is limited to the plate at ambient temperature, thus avoiding heat transfer effects not related to the effectiveness of the model.

Details of the test cases used for the comparison between numerical and experimental data are reported in Table 5. The computational domain used for the simulations is a $70 \times 70 \times 25\ \mathrm{mm}^3$ structured grid with 0.5 mm spacing, fine enough to reduce the grid-size sensitivity of less than 1% in terms of spray penetration. The spray initiation is based on the measured needle opening and closure times. The fuel flow rate law is made up of three strokes: two for the opening and closure phases at constant slope and one stroke with constant fuel flow rate. A total of 10,000 sample parcels are introduced during the injection time.

Fig. 13 shows the comparison between the experimental and numerical spray tip penetration with a back-pressure of 0.1 MPa. A good agreement between numerical and experimental results is observed. It is worth

Table 5
Selected test cases

Case #	Injection pressure [MPa]	Back-pressure [MPa]
1	80	0.1
2		1
3		3
4		5
5	120	0.1
6		1
7		3
8		5

noting that it is not possible to discriminate penetration regimes, due to the very high injection pressure and the very low back-pressure.

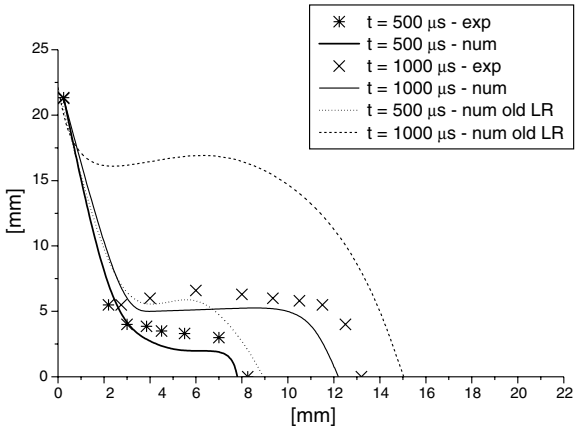

Fig. 14. Profiles of the spray wall-impingement at different time from SOI: experimental–numerical original model–numerical modified model comparison $p_{inj} = 120$ MPa, $p_{ch} = 5$ MPa.

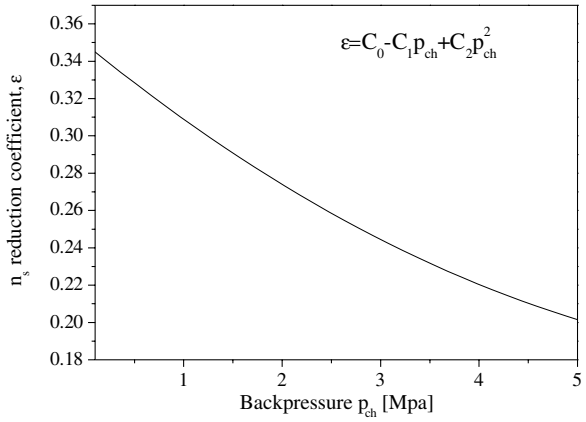

Fig. 15. Relationship between the number of splashed droplets reduction coefficient and back-pressure.

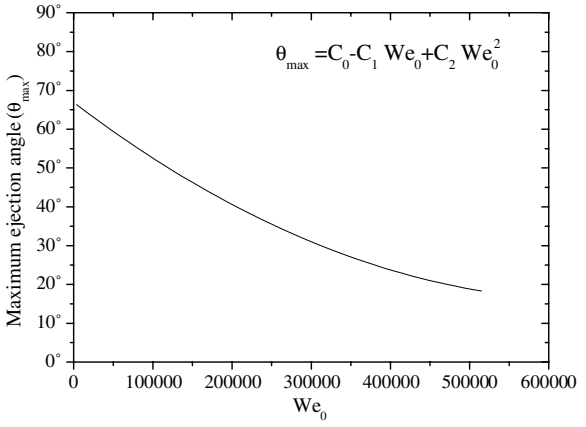

Fig. 16. Relationship between the maximum ejection angle and the impinging droplet normal Weber.

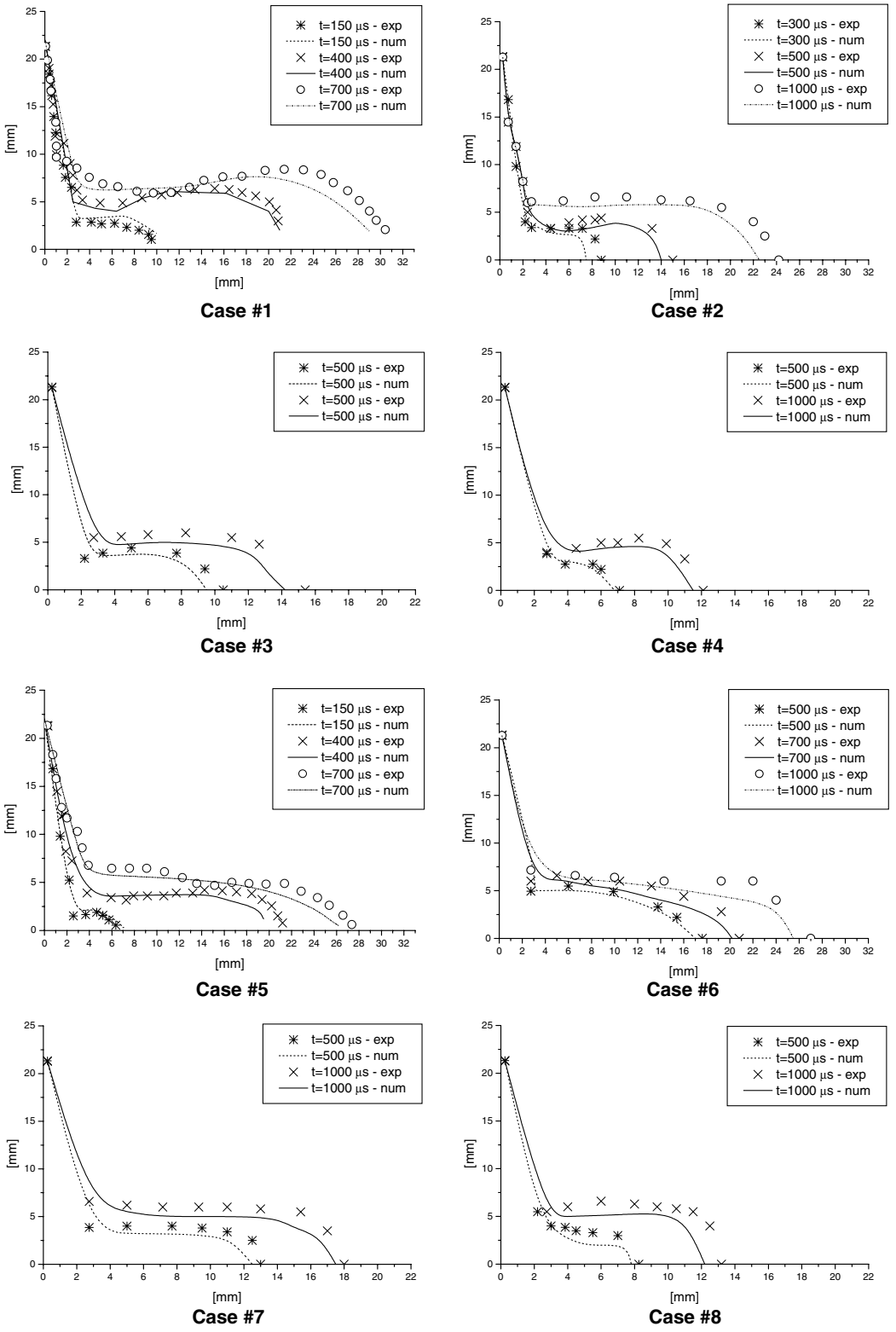

Fig. 17. Profiles of the spray wall-impingement at different time from SOI for the operating conditions listed in Table 5: experimental–numerical comparison.

7.1. New Splash model

Despite the acceptable results obtained up to 300 bar of injection pressure, the original version of the LR model does not reproduce the splash phenomenon at the present experimental conditions. An example is given in Fig. 14, which shows an overestimation of the thickness and an underestimation of the radial extension of the splash cloud for an injection pressure of 120 MPa and a back-pressure of 5 MPa.

The inability of reproducing the splash phenomenon can be related to the number of secondary droplets generated by the spray–wall interaction (and then to the secondary droplets dimension) and to the tangential component of the splashed droplets velocity.

The number of splashed droplets, in fact, is given in function of the Weber number by the experimental correlation of Naber and Farrel (1993). However, this correlation is extrapolated for a low velocity impinging spray. At high injection pressures this gives very small low-penetrating splashed droplets, thus resulting into an underprediction of the splash cloud radius. Therefore, the LR model has been modified by reducing the number of splashed droplets and relating them to the back-pressure as reported in Fig. 15.

The calculation of the tangential component of the splashed droplets velocity is based on a theoretical correlation resulting from the analysis of a low velocity impinging single droplet. However, the experimental results demonstrate that the effects of a spray droplet impacting onto a fluctuating film or a dry wall significantly differ from those of a single droplet impacting onto a stationary, uniform film. Therefore, the direction of the splashed droplets velocity has been calculated by defining the ejection angle range as a function of the impinging droplet normal Weber number in order to keep into account the different operating conditions in terms of injection pressure and back-pressure. Employing a function of the droplet normal Weber number should generalise the model, as the spray characteristics before impingement are determined by multiple factors (i.e. injection and chamber gas pressure, orifice characteristics).

The employed relationship between the maximum ejection angle, θ_{max}, and We_0 is reported in the graph of Fig. 16. These changes, determined on the basis of the present measurements, allow reproducing with a good accuracy the experimental splash cloud produced by Diesel-like high pressure sprays with different back-pressures. A good agreement between numerical and experimental splash height and radial width can be observed in Fig. 17 that shows the spray profiles after wall-impingement at different times after SOI for the test cases reported in Table 5. A further confirmation of the effectiveness of the new splash model is given in Figs. 18 and 19, where the numerical splash cloud is overimposed on the experimental one at different injection pressures and back-pressures ($p_{inj} = 120$ MPa and $p_{ch} = 1$ MPa for Fig. 17, $p_{inj} = 80$ MPa and $p_{ch} = 3$ MPa for Fig. 18). In this way, it is possible to appreciate the agreement between numerical and experimental images even under significantly different operating conditions.

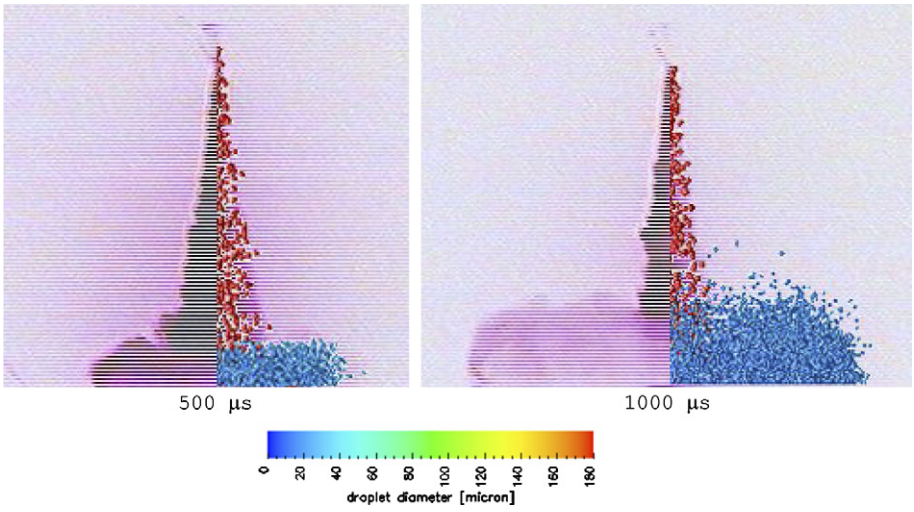

Fig. 18. Numerical and experimental time evolution of the spray: $p_{inj} = 120$ MPa, $p_{ch} = 1$ MPa, $T_w = 298$ K.

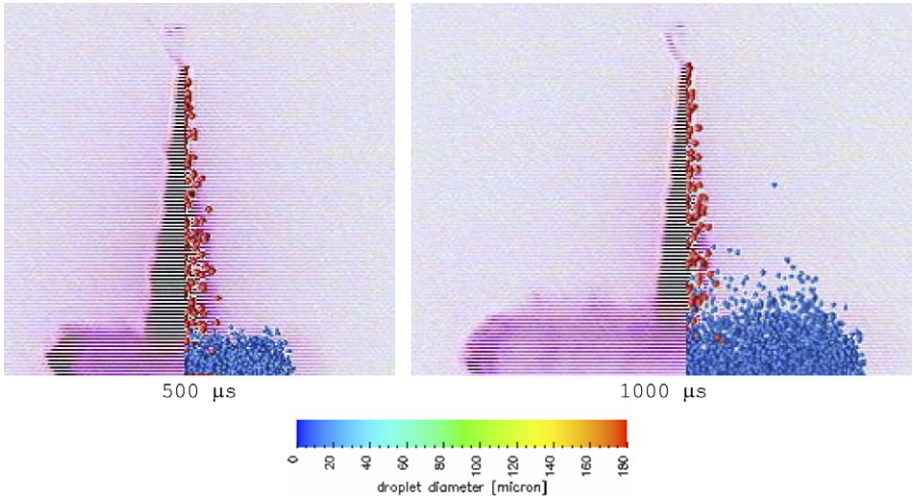

Fig. 19. Numerical and experimental time evolution of the spray: $p_{inj} = 800$ MPa, $p_{ch} = 3$ MPa, $T_w = 298$ K.

The impinging-spray image processing of Fig. 12 highlights higher density values of the particles in the impact zone and/or nearest it and shows the propagation of the ''wall-main jet'' region outward at increasing time from the SOI. This constitutes the ''wall-main jet'' region with density values comparable to the ''main jet'' region of free running spray. The rebounded droplets move both radially and axially (in opposite versus to the incoming spray) going into new rebounding and constructing the fuel layer on the wall. Then, far from the impact point, a ''mixing'' region is identified where relatively large droplets interact with the gas and curls and vortexes appear. Finally, a ''stagnate'' region in the interface between the incoming primary spray and the outward travelling fuel can be detected. Here the layer thickness is sensibly lower defining an upper limit to the rebounding angle from the plate.

It is interesting to notice how this last experimental observation is completely confirmed by the flow field evaluated by the KIVA 3 V code. In Fig. 20, in fact, the flow field and the particle distribution predicted by the enhanced version of the BG model at 1200 μs after the SOI for an injection pressure of 120 MPa and a

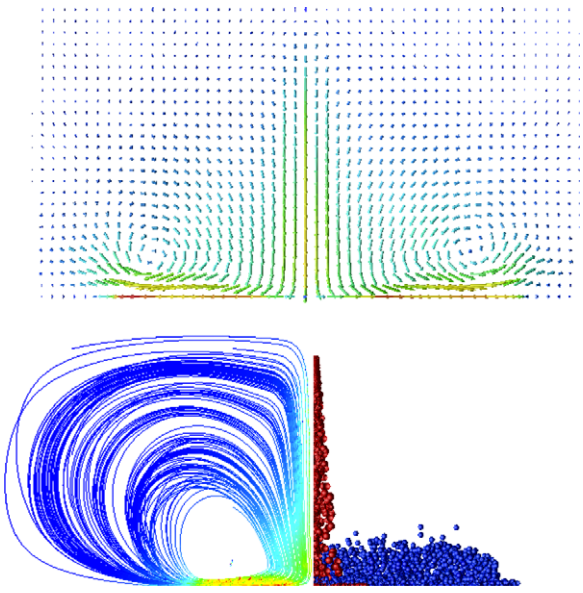

Fig. 20. Numerical flow field during the injection process.

back-pressure of 0.1 MPa are reported. All the spray characterizing regions (stagnation region, mixing region, etc.) are observable as well as the formation of two roll-up vortices at the spray wall-jet after impingement.

8. Conclusions

In this paper the impingement of a high pressure diesel spray on a flat wall is studied both numerically and experimentally.

The analysis has been carried out at two injection pressures, 80 and 120 MPa and three back-pressures, 1.0, 3.0 and 5.0 MPa, covering typical diesel gas density in the combustion chamber in all operative conditions. The fuel impacts on the plate at temperatures varying from 20 °C to 500 °C, for atmospheric gas pressure, and to 300 °C for a back-pressure up to 5.0 MPa.

The results of the experimental analysis allow to draw the following conclusions:

1. The pressure of the gas in the vessel significantly influences the geometry of the scattered parcels after the impact, producing a high compression of less dense and highly atomized zone at increasing back-pressures.
2. The injection pressure has a significant effect on the radial growth and the splash height of the secondary droplets cloud.
3. The wall temperature effect on the radial growth and the thickness of the splash cloud highlights an important role of the heat exchange between the droplets and the wall. The thickness, in fact, presents a minimum at around 100 °C for both 120 MPa and 80 MPa of injection pressure. However, only for the latter an absolute maximum is observed at about 450 °C. This particular behaviour could be related to a combined effect of Nukiyama and Leidenfrost effects.
4. Through an image post-processing procedure it is possible to relate the light intensity to the fuel spray particle concentration, thus allowing to highlight the shifting of the highest density areas from the impacting zone toward outside at increasing time from the SOI. This tool provides valuable information on the fuel-air mixing process, which is in turn vital for the optimisation of the combustion process in high-speed Diesel engines.

The experimental results for the cold plate have been used to develop and validate a phenomenological splash model to be implemented in a multi-dimensional code for high speed Diesel engines simulation, being the models available in literature applicable only to low injection pressures and, often, related to single-droplet empirical data.

The present model is a modified version of the one proposed by Lee et al. (2000, 2001). The original version of this model well behaves for low injections pressures but fails to reproduce the spray impingement phenomena at the injection pressures typical of modern Diesel engines. The weakness of this model can be brought back to the experimental correlations used to determine the number of the secondary droplets and their tangential velocity. Those empirical correlations, in fact, refer to experimental data on low velocity single droplet or spray impingement processes that do not take into account a back-pressure higher than 0.1 MPa. The model has been then modified by applying two correlations based on the experimental data provided in this paper:

– a correlation between the secondary droplets ejection angle and the impinging droplet Weber number;
– a correlation between the number of secondary droplets and the back-pressure.

The new model, based on the conservation laws and on the present experimental results, demonstrates to be capable of predicting the transient behaviour of high velocity impinging sprays. Nevertheless a further research is still needed to analyse and model the spray–wall interaction at high temperatures when fuel evaporation may significantly affect the overall phenomenon. The applicability to different fuels (i.e. gasoline) will be also studied. This numerical tool is essential to accurately model the thermo-fluid dynamics in modern Diesel engines as the post-impingement characteristics play a fundamental role on the air–fuel mixing process and on the consequent combustion event.

References

Allocca, L., Amato, U., Bertoli, C., Corcione, F.E., 1990. Comparison of models and experiments for diesel fuel sprays. In: COMODIA 1990, Int. Symposium on Diagnostic and Modelling of Combustion in IC Engines, Kyoto, Japan, pp. 225–261.

Allocca, L., Corcione, F.E., Golini S., Papetti, F., 1993. Assessment of wall heat transfer model for an impinging diesel spray. In: ASME Conference, August 8–11,1993, Atlanta, GA.

Allocca, L., De Vita, A., Di Angelo, L., 2002. Wall-impingement analysis of a spray from a common rail injection system for diesel engines. THIESEL 2002, Valencia (Spain), pp. 67–76.

Allocca, L., Alfuso, S., Corcione, F.E., 2003. Assessment of dynamic performances of diesel solenoid injectors for a multiple injection common rail system. SAE_NA Paper 2003-01-21.

Allocca, L., Andreassi, L., Ubertini, S., 2006a. Evaluation of splash models with high-pressure diesel spray. SAE Technical Paper 2006-01-1117.

Allocca, L., Andreassi, L., Ubertini, S., 2006b. Enhanced splash models for high pressure diesel sprays. ASME ESDA 2006-01-1117.

Amagai, K., Arai, M., 2004. Evaporation and fuel vapour distribution in a diesel spray impinging on a hot wall. COMODIA 2004, August 2–5, 2004, Yokohama, Japan.

Andreassi, L., Ubertini, S., 2005. Multidimensional modeling of spray impingement in modern diesel engines. SAE Technical Paper 2005-24-092.

Arcoumanis, C., Chang, J.C., 1994. Flow and heat transfer characteristics of impinging transient diesel sprays. SAE Technical Paper 940678.

Bai, C., Gosman, A.D., 1995. Development of Methodology for Spray Impingement Simulation. SAE Technical Paper 950283.

Bella, G., Rotondi, R., Corcione, F., Valentino, G., 1999. Experimental and numerical analysis of a diesel spray. In: Proceedings of ICE 1999.

Bella, G., Rocco, V., Ubertini, S., 2002. Combustion and spray simulation of a DI turbocharged diesel engine. Journal of Engines – SAE Transactions 2002, 2549–2565.

Chaves, H., Knapp, M., Kubitzek, A., Obermeier, F., 1995. Experimental study of cavitation in the nozzle hole of diesel injectors using transparent nozzles. SAE Technical Paper 950290.

Cossali, G.E., Marengo, M., Santini, S., 2005. Secondary atomization produced by single drop vertical impacts onto heated surfaces. Experimental Thermal and Fluid Science, published online.

De Vita, A., Di Angelo, L., Allocca L., 2002. Early injection and time-resolved evolution of a spray for GDI engines. ASME Fluids Engineering Division Summer Meeting, Montreal.

Di Stasio, S., Allocca, L., 2000. Influence of the gas ambient nature on diesel spray properties at high injection pressure: experimental results. THIESEL 2000, Valencia (Spain).

Eckause, J.E., Reitz, R.D., 1995. Modeling heat transfer to impinging fuel sprays in direct-injection engines. Atom. Sprays 5, 213–242.

Fujimoto, H., Senda, J., Nagae, M., Hashimoto, A., Saito, M., Katsura, N., 1990. Characteristics of a diesel spray impinging on a flat wall. In: Proceedings of COMODIA 90 Int. Symposium on Diagnostic and Modeling of Combustion in I.C. Engines, Kyoto, Japan, pp. 193–198.

Fujimoto, H., Hyun, G., Nogami, M., Hirakawa, K., 1997. Impinging gas jets by means of image processing. SAE Paper 970045.

Grover, R.O. Jr., Assanis, D.N., 2001. A spray wall impingement model based upon conservation principles. In: Fifth International Symposium on Diagnostics and Modeling of Combustion in Internal Combustion Engines, pp. 551–559.

Guerrassi, N., Champoussin, J.C., 1996. Experimental study and modeling of diesel spray/wall impingement. SAE Technical Paper 960864.

Hu, K., Gosman, A.D., 1991. A phenomenological model of diesel spray atomization. In: Proceedings of the International Conference on Multiphase Flows, Tsukuba, Japan.

Ibrahim, E.A., Yang, H.Q., Przekwas, A.J., 1993. Modeling of spray droplets deformation and breakup. AIAA J. Propulsion Power 9, 651–654.

International Organization for Standardization, 1988. Road vehicles – Calibration fluid for diesel injection equipment, ISO 4113.

Katsura, N., Saito, M., Senda, J., Fujimoto H., 1989. Characteristics of a Diesel spray impinging on a flat wall. SAE Technical Paper 890264.

Lee, S., Ryou, H., 2000. Modeling of spray–wall interactions considering liquid film formation. In: Proceedings of the Eight International Conference on Liquid Atomization and Spray Systems, Pasadena, CA, pp. 586–593.

Lee, S., Ko, G.H., Ryou, H., Hong, K.B., 2001. Development and application of a new spray impingement model considering film formation in a diesel engine. KSME Int. J. 15, 951–961.

Lopez, J.J., Pickett, L.M., 2004. Jet/wall interaction effects on soot formation in a diesel fuel jet. COMODIA 2004.

Marengo, M., Steigleder, T., Tropea, C., 1996. Aufprall von tropfen auf flussigkeitsfilmen. Workshop ueber Sprays, Erfassung von Spruhvorgangen und Techniken der Fluidzerstaubung, A 3-1 – A 3-8.

Mills, A.A., Fry, J.D., 1982. Rate of evaporation of hydrocarbons from a hot surface: Nukiyama and leidenfrost temperatures. Eur J. Phys., 3152–3154.

Moita, A.S., Moreira, A.L., 2005. The interaction of fuel droplets with heated nterposed surfaces in IC engines. SAE Paper 2005-25-084.

Mundo, C., Sommerfeld, M., Tropea, C., 1995. Droplet-wall collisions: experimental studies of the deformation and breakup process. Int. J. Multiphase Flow 21, 151–173.

Mundo, C., Sommerfeld, M., Tropea, C., 1996. Spray wall impingement phenomena: experimental investigations and numerical predictions. In: 12th Annual Conference of ICLASS Europe, Lund, Sweden, pp. 19–21.

Naber, J.D, Farrel, P.V., 1993. Hydrodynamics of Droplet Impingement on a Heated Surface. SAE Technical. Papers 930919.
Naber, J.D., Reitz, R.D., 1988. Modeling engine/spray wall impingement. SAE Technical Paper 881316.
O'Rourke, P.J., Amsden, A.A., 1987. The Tab Method for Numerical Calculation of Spray Droplet Breakup. SAE Technical Paper 872089.
O'Rourke, P.J., Amsden, A.A., 1996. A Particle Numerical Model for Wall Film Dynamics in Port-Injected Engines. SAE Technical Paper 961961.
O'Rourke, P.J., Amsden, A.A., 2000. A Spray/Wall Interaction Submodel for the KIVA-3V Wall Film Model. SAE Technical Paper 2000-01-0271.
Patterson, M.A., Reitz, R., 1998. Modeling the Effects of Fuel Spray Characteristics on Diesel Engine Combustion and Emission. SAE Technical Paper 980131.
Reitz, R.D., Diwakar, R., 1987. Structure of High Pressure Fuel Sprays. SAE Technical Paper 870598.
Roisman, I.V., Tropea, C., 2005. Fluctuating flow in a liquid layer and secondary spray created by an impacting spray. Int. J. Multiphase Flow 31, 179–200.
Saito, A., Kawamura, K., Watanabe, S., Takahashi, T., Tuzuki, N., 1993. Analysis of impinging spray characteristics under high-pressure fuel injection (1st report, measurements of impinging spray characteristics). Trans. Jap. Soc. Mech. Eng., Part B 59, 3290–3295.
Sarre, C. von K. , Kong, S.C., Reitz, R.D., 1999. Modeling the Effects of Injector Nozzle Geometry on Diesel Sprays. SAE Technical Paper 1999-01-0912.
Stanton, D.W., Rutland, C.J., 1996. Modelling Fuel Film Formation and Wall Interaction in Diesel Engines. SAE Technical Paper 960628.
Ubertini, S., Mariani, F., Postrioti, L., 2004. Experimental Validation of a Spray Breakup Model in High Pressure Ambient Conditions. Selected papers from the THIESEL 2002, 61–86, Springer Verlag Book.
Wachters, L.H.J., Westerling, N.A.J., 1966. The heat transfer from a hot wall to impinging water drops in the spheroidal state. Chem. Eng. Sci. 21, 1047–1056.
Wang, D.M., Watkins, A.P., 1993. Numerical modeling of diesel spray impinging on flat walls. Int. J. Heat Fluid Flow 14, 301–312.
Winterbone, D.E., Yates, D.A., Clough, E., Rao, K.K, Gomes, P., Sun, J.H., 1994 Quantitative analysis of combustion in high-speed direct injection Diesel engines. COMODIA 94 Yokohama, Japan.
Wu, Z., 1992. Modélisation et Calcul Implicite Multidomaine d'Ecoulements Diphasiques Gas-Gouttelettes. Ph.D. Thesis, Université Pierre et Marie Curie, Paris, France, 1992.
Xiong, T.Y., Yuen, M.C., 1991. Evaporation of a liquid droplet on a hot plate. Int. J. Heat Mass Transf. 34, 1881–1894.
Yarin, A.L., Weiss, D.A., 1995. Impact of drops on solid surfaces: self-similar capillary waves, and splashing as a new type of kinematic discontinuity. J. Fluid Mech. 283, 141–173.